

The Growth Rate of Supermassive Black Holes and Its Dependence on the Stellar Mass of Galaxies at the Present Epoch

Sergey A. Prokhorenko^{2,1*}, Sergey Yu. Sazonov¹

¹ Space Research Institute of the Russian Academy of Sciences (IKI), 84/32 Profsoyuznaya Str, Moscow, Russia, 117997

² National Research University «Higher School of Economics», Pokrovsky Bulvar 11, 101990 Moscow, Russia

Abstract — We study the distribution of accretion rates onto supermassive black holes in AGNs of the local Universe ($z < 0.15$) based on near-infrared and hard X-ray surveys (2MASS and Swift/BAT). Using sufficiently accurate black hole mass estimates, we reliably estimated the Eddington ratio, λ_{Edd} , for approximately half of the objects in the AGN sample; for the remaining ones we used a rougher estimate based on the correlation of M_{BH} with the galaxy stellar mass M_* . We found that for a wide range of galaxy masses, $9.28 < \log(M_*/M_\odot) < 12.28$, including the most massive galaxies in the local Universe, the distribution $f(\lambda_{\text{Edd}})$ above $\log \lambda_{\text{Edd}} = -3$ can be described by a power law with M_* -independent parameters, declining with a characteristic slope ≈ 0.7 up to the Eddington limit ($\log \lambda_{\text{Edd}} \sim 0$), where there is evidence for a break. In addition, there is evidence that at $\log \lambda_{\text{Edd}} < -3$ the dependence $f(\lambda_{\text{Edd}})$ has a lower slope or flattens out. The mean characteristic growth time of supermassive black holes at the present epoch turns out to depend weakly on the galaxy stellar mass and to exceed the lifetime of the Universe, but by no more than one order of magnitude. The mean duty cycle of supermassive black holes (the fraction of objects with $\lambda_{\text{Edd}} > 0.01$) in the local Universe also depends weakly on M_* and is 0.2–1%. These results obtained for the present epoch confirm the trends found in previous studies for the earlier Universe and refine the parameters of the dependence $f(\lambda_{\text{Edd}}|M_*)$ at $z < 0.15$. The revealed universal (weakly dependent on the galaxy stellar mass) pattern of the dependence $f(\lambda_{\text{Edd}})$ probably stems from the fact that, at present, the episodes of mass accretion onto supermassive black holes are associated mainly with stochastic processes in galactic nuclei rather than with global galaxy evolution processes.

Keywords: supermassive black holes, accretion, active galactic nuclei, X-ray sources, luminosity function.

1 INTRODUCTION

The nucleus of almost every galaxy at the present epoch is currently believed to host a supermassive black hole (SMBH). A correlation between the black hole (BH) mass M_{BH} and such characteristics of the galaxy central stellar bulge as the bulge mass M_b and the velocity dispersion σ has been revealed (Magorrian et al. 1998; Tremaine et al. 2002; for a review, see Kormendy and Ho 2013). This suggests that the star formation in galaxies and the growth of their central BHs could correlate closely with each other during the evolution of the Universe. In particular, the feedback mechanisms associated with huge energy release during mass accretion onto SMBHs could play a prominent role (see, e.g., Ciotti and Ostriker 2001; Di Matteo et al. 2005; Murray et al. 2005; Sazonov et al. 2005; for a review, see also Fabian 2012; King and Pounds 2015; Naab and Ostriker 2017), despite the fact that the BH mass typically accounts for only 10^{-3} – 10^{-2} of the bulge mass and the region of its gravitational influence extends only to the galactic nucleus. However, it is also clear that this correlation is not simple, as suggested, in particular, by the detection of SMBHs in galaxies with pseudo-bulges and without bulges altogether (Kormendy and Ho 2013).

It is impossible to get a fairly comprehensive idea of the correlation between SMBH growth and galaxy evolution using individual objects as an example because of the huge (up to the cosmologi-

cal ones) time scales on which these processes occur. Therefore, it is necessary to resort to statistical studies of galaxies and active galactic nuclei (AGNs). Such studies have been carried out particularly actively in the last two decades owing to the appearance of sufficiently deep surveys in various wavelength ranges. It has been realized that the main growth of SMBHs in the Universe occurred at redshifts $z \sim 1$ – 3 (see, e.g., Ueda et al. 2014; Aird et al. 2015), approximately at the same epoch when the stars in galaxies were formed most actively (for a review, see Madau and Dickinson 2014), while at a later time both these processes slowed down considerably. At the same time, starting from $z \sim 3$ and up until now the integrated mass accretion rate onto BHs in galactic nuclei was approximately proportional to the total star formation rate in the Universe (see, e.g., Merloni and Heinz 2008; Shankar et al. 2009). However, these trends have been reliably established only for the Universe on average, while much remains unclear in the evolution of galaxies of various types and the growth of their central BHs.

Most of the key questions remain open even for the present epoch. For example, why are some galaxies active (in particular, the Seyfert ones), while others not? To what extent is this associated with the processes occurring in the central region of the galaxy and with the evolution of the galaxy as a whole? What is the characteristic AGN duty cycle? A possible way of searching for answers to these questions is a statistical study of the occurrence of AGNs with different luminosities (i.e., with different accretion rates onto

* E-mail: sprokhorenko@iki.rssi.ru

SMBHs) in galaxies of different types. In this case, the stellar mass M_* can be used as a key characteristic of galaxies.

One of the first such studies was carried out by Aird et al. (2012). A representative sample of $\sim 25 \times 10^3$ galaxies, among which there were ~ 200 X-ray-selected AGNs at redshifts $0.2 < z < 1.0$, was produced in several small sky fields (with a total area $\sim 3 \text{ deg}^2$). For all of the AGNs the accretion rate onto the SMBH was estimated (from the measured X-ray luminosity), while for all of the galaxies (including the AGNs) the BH mass was roughly estimated under the assumption that $M_{\text{BH}} = 0.002 M_*$ (assuming the bulge to dominate in the total galaxy stellar mass). As a result, the distribution of SMBHs in Eddington ratio λ_{Edd} (the ratio of the accretion rate to the critical one specified by the Eddington luminosity) was studied, and this dependence [$f(\lambda_{\text{Edd}})$] turned out to have a falling power-law shape with a slope of about -0.65 , which does not depend on M_* , and a normalization that increases with z . Thus, evidence that the SMBH growth is universal in galaxies of different masses and that it dramatically slowed down in the Universe as a whole between the epochs $z = 1$ and $z = 0.2$ was found.

Bongiorno et al. (2012) obtained results similar to those in Aird et al. (2012), but for the earlier Universe, $0.3 < z < 2.5$, and pointed out that there is no dependence of the λ_{Edd} distribution not only on the mass, but also on the star formation rate; furthermore, a break in the power-law dependence $f(\lambda_{\text{Edd}})$ was detected at $\lambda_{\text{Edd}} \sim 1$. Subsequently, Bongiorno et al. (2016) refined the shape of this break and its evolution with redshift, while Georgakakis et al. (2017) detected a flattening or, possibly, a break of the function $f(\lambda_{\text{Edd}})$ at $\log \lambda_{\text{Edd}} \lesssim -3$ and pointed out some dependence of $f(\lambda_{\text{Edd}})$ on M_* , whereby low accretion rates (λ_{Edd}) dominate among massive galaxies. Finally, while studying the Universe in a wide range of redshifts, $0.1 < z < 4$, Aird et al. (2018), on the whole, confirmed and refined these trends.

In all of the mentioned papers the conclusions about the distribution of accretion rates onto SMBHs were drawn from a “specific accretion rate”, i.e., the ratio of the AGN X-ray luminosity to the total host galaxy stellar mass. However, since the correlation between M_{BH} and M_* is weak, the specific accretion rate is only a rough approximation of λ_{Edd} . Furthermore, because of the limited area of the X-ray surveys (no more than $\sim 10^3 \text{ deg}^2$) used in these studies, the range of their redshift coverage begins from $z \sim 0.1$ – 0.2 , i.e., the present-day Universe turned out to be least studied.

Hence, it should be noted that the dependence $f(\lambda_{\text{Edd}})$ at the present epoch was studied in Kauffmann and Heckman (2009), where the selection of AGNs, only type 2 ones, was based not on X-ray surveys, but on the optical Sloan Digital Sky Survey (SDSS). More specifically, AGNs were selected by their emission in narrow emission lines, while their bolometric luminosities (and, as a consequence, accretion rates) were estimated from the flux in the narrow [OIII] $\lambda 5007$ line. The initial conclusions of this paper differed radically from those of the studies listed above, which are based on the X-ray selection of AGNs. Subsequently, however, Jones et al. (2016) showed that strong selection effects arise in this method, while after the correction for them the results based on SDSS agree satisfactorily with the fact that the dependence $f(\lambda_{\text{Edd}})$ (at low redshifts) has a power-law shape with an exponential cutoff at $\lambda_{\text{Edd}} \sim 1$.

The goal of this paper is to study the λ_{Edd} distribution of

SMBHs and its dependence on M_* at the present epoch ($z < 0.15$). To systematically consider as many AGNs in the local Universe as possible, we will rely on two all-sky surveys: (1) the 2MASS near-infrared photometric survey to construct a large sample of galaxies ($\sim 10^6$ objects) with known redshifts and (2) the hard X-ray survey with the BAT instrument onboard the Neil Gehrels observatory to construct a sample of AGNs (~ 650 objects). Using the near-infrared survey allows the galaxy stellar masses to be estimated fairly accurately, while using the hard X-ray survey minimizes the influence of selection effects when selecting AGNs. Apart from rough SMBH mass estimates based on the correlation with the stellar bulge mass, we also use more accurate M_{BH} estimates available approximately for half of our AGN sample. As far as we know, such a study is carried out for the first time for the local Universe.

2 SELECTION OF OBJECTS FOR THE STUDY

2.1 Galaxy Sample

The Two Micron All Sky Survey (2MASS) (Skrutskie et al. 2006) makes it possible to produce a large homogeneous sample of galaxies in the relatively nearby Universe and to estimate quite reliably their stellar masses based on photometric measurements in the K_s band ($\lambda = 2.159 \mu\text{m}$, $\Delta\lambda = 0.262 \mu\text{m}$)¹. To measure the galaxy luminosities in this band, we used the 2MRS (Huchra et al. 2012) and 2MPZ (Bilicki et al. 2013) catalogs of galaxy redshifts from 2MASS. Spectroscopic redshift measurements are presented in the 2MRS catalog; in the 2MPZ catalog there are no spectroscopic redshift estimates for most of the objects, but there are photometric z estimates found with machine learning algorithms. Although such estimates are characterized by significant errors, they are well suited for our purposes, given the more serious assumptions that we have to make in the course of our study.

Having cross-correlated the 2MRS (43533 galaxies) and 2MPZ (934175 galaxies) catalogs, we ascertained that the 2MPZ catalog lacks 4454 galaxies that are present in the 2MRS catalog. Therefore, to increase the statistical completeness of the galaxy sample, it is necessary to use the combined 2MRS/2MPZ catalog. We excluded the sky region near the Galactic plane ($|b| < 10^\circ$) from consideration, because in this zone the 2MRS and 2MPZ catalogs of galaxies are characterized by an insufficient completeness. In addition, we imposed a constraint in redshift, $z < 0.15$. This was done again because of the need to provide a high statistical completeness of the sample and to be able to neglect the influence of the cosmological evolution of the galaxy population on the results of our study.

The above constraints ($|b| > 10^\circ$ and $z < 0.15$) are satisfied by 793289 galaxies from the combined 2MRS/2MPZ catalog.

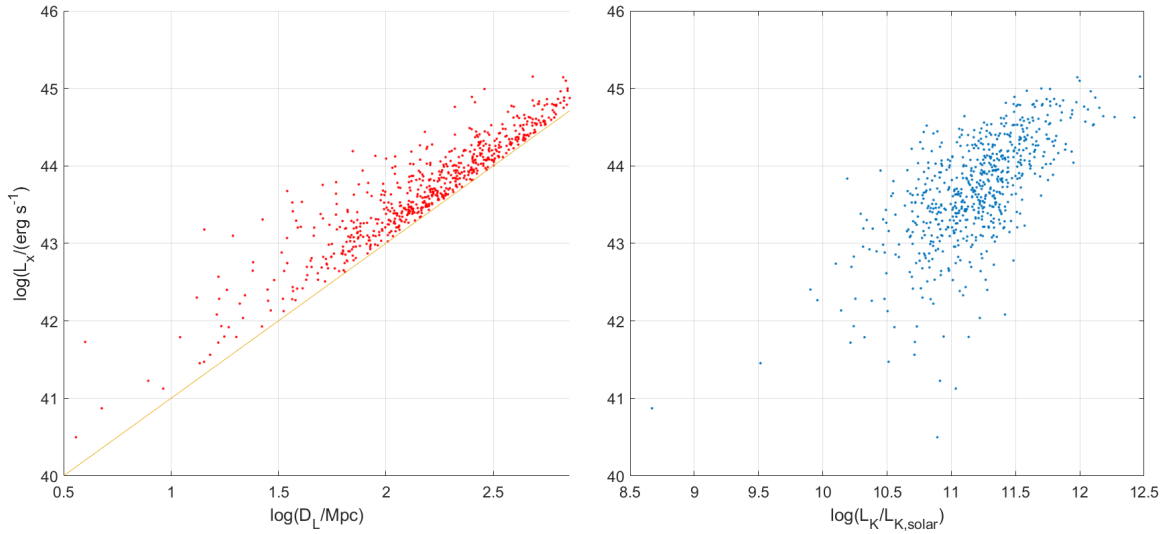
2.2 AGN Sample

To produce a sample of AGNs, we used the currently deepest available and homogeneous, over most of the sky, catalog of hard X-ray (14–195 keV) sources detected by the BAT instrument onboard the

¹ Below K_s will be abbreviated to K , despite the fact that it is customary to consider a different band close in wavelength (centered at $\lambda = 2.2 \mu\text{m}$) to be the K band

Table 1. Distribution of AGNs in types and sources of information about the redshift/distance

Type	Total	Present in 2MPZ+2MRS	Spectroscopic z	Photometric z	Accurate distances
Seyfert I	246	205	242	4	4
Seyfert II	353	339	343	10	41
LINER	5	5	5	0	1
Unknown AGN	49	48	29	20	1
Total:	653	597	619	34	47

**Figure 1.** Left: X-ray luminosity (14–195 keV) versus distance from the Swift/BAT AGN sample. The orange line indicates the luminosity threshold corresponding to the minimum X-ray flux for an AGN to be included in the sample ($F_{\min} = 8.4 \times 10^{-12} \text{ erg s}^{-1} \text{ cm}^{-2}$). Right: The distribution of AGNs in X-ray luminosity and K -band luminosity.

Swift observatory (Swift/BAT). From the latest published version of the catalog based on the first 105 months of Swift/BAT observations (Oh et al. 2018) we selected AGNs with fluxes above $8.4 \times 10^{-12} \text{ erg s}^{-1} \text{ cm}^{-2}$ (14–195 keV). At such a depth 90% of the sky was covered (all sky was covered with a sensitivity better than $9.3 \times 10^{-12} \text{ erg s}^{-1} \text{ cm}^{-2}$). Similarly to the galaxy sample, we imposed the constraints $|b| > 10^\circ$ and $z < 0.15$ on the AGN sample as well. This choice additionally stems from the fact that a significant fraction of the Swift/BAT X-ray sources at low Galactic latitudes remain unidentified.

From the Swift/BAT catalog we took only objects with the Seyfert I (Sy 1.0–1.8), Seyfert II (Sy 1.9–2.0), LINER, and Unknown AGNs (i.e., Seyfert galaxies and AGNs of an uncertain optical type) types and excluded blazars (Beamed AGNs), because this is a peculiar class of AGNs with highly collimated emission toward the observer, which requires a separate consideration.

Thus, we selected 653 AGNs.

2.3 Overlap between the Galaxy and AGN Samples

Having cross-correlated the Swift/BAT AGN sample and the 2MRS/2MPZ galaxy sample, we found 597 matches (the controversial cases were resolved manually using the NASA/IPAC Extra-

galactic Database (NED)). For 43 of these objects we refined the K -band fluxes using the 2MASS Large Galaxy Atlas (Jarrett et al. 2003), because it contains more accurate measurements of the IR fluxes for nearby galaxies.

For the remaining 56 AGNs (which are absent in the 2MRS and 2MPZ catalogs) the K -band flux was taken from the 2MASS Extended Catalog (Jarrett 2004) — 14 objects, the 2MASS All-Sky Catalog of Point Sources (Cutri et al. 2003) — 41 objects, and the 2MASS Large Galaxy Atlas — 1 object (a galaxy from the constellation Circinus).

2.4 Distances to Objects

The galaxy and AGN redshifts were taken from the 2MRS and 2MPZ catalogs using (if available) the spectroscopic measurements and giving preference to the 2MPZ catalog. For those AGNs that are absent in the 2MRS and 2MPZ catalogs we used the redshifts given in the original catalog of the 105-month Swift/BAT survey. Note that the choice of a redshift source is of no fundamental importance for the problem under consideration, because the spectroscopic redshifts given in the Swift/BAT and 2MPZ catalogs differ, on average, by 1.5% and by more than 10% only in five cases (in these cases we took the estimates from NED). The difference between the

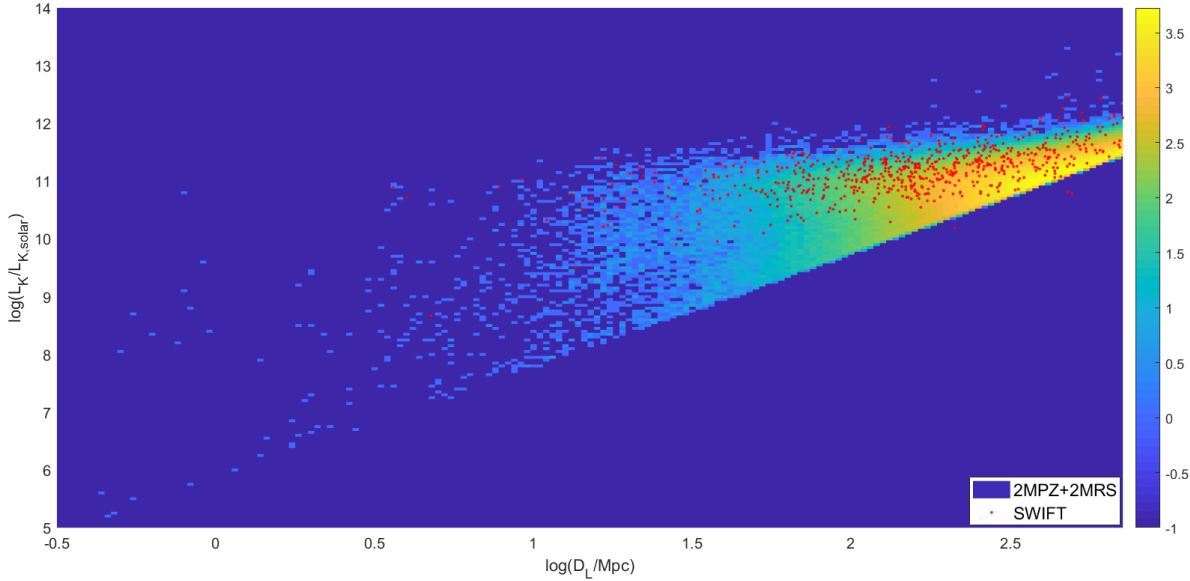


Figure 2. K -band luminosity of the galaxies from the 2MRS/2MPZ sample (in solar luminosities in the same band) versus distance. The field was divided into intervals with a width of 0.02 order of magnitude along the distance axis and 0.05 order of magnitude along the luminosity axis. The color indicates the common logarithm of the number of galaxies that fell into a given region of the diagram (in accordance with the color scale on the right). The value of the logarithm -1 means that no galaxy fell into a given region. The red dots mark the AGNs from the Swift/BAT sample.

Swift/BAT and 2MRS redshifts for the AGN sample is, on average, 1% and does not exceed 7% (in all but one case, it is less than 5%). For the AGN sample we took a total of 399 spectroscopic and 34 photometric z from the 2MPZ catalog and used the spectroscopic z from the 105-month Swift/BAT catalog for the remaining 220 objects.

For most of the galaxies and AGNs the photometric distances and, as a consequence, the luminosities were calculated from the redshifts. In this case, we used the cosmological model with $\Omega_0 = 0.3$ and $h_0 = 70 \text{ km s}^{-1} \text{ Mpc}^{-1}$. For 47 nearest AGNs $z \lesssim 0.01$ we used more accurate distance estimates from the Cosmicflows3 database (Tully et al. 2016). Similarly, after the correlation of the 2MRS and 2MPZ catalogs with Cosmicflows3, we corrected 8625 of the 42 533 and 7241 of the 934 175 distances to the galaxies in these catalogs, respectively.

Thus, for all 653 AGNs in the sample we found their counterparts in 2MASS, the corresponding K -band fluxes, and the distances. Information about the optical types and redshifts/distances of the AGNs in the sample is summarized in Table 1.

3 PROPERTIES OF THE GALAXY AND AGN SAMPLES

Figure 1(left) shows the distribution of AGNs from the sample under study in X-ray luminosity L_X (in the 14–195 keV energy band) and distance. Figure 1(right) presents the distribution of these AGNs in X-ray luminosity and K -band luminosity L_K . Here and below, the K -band luminosities of the objects are expressed in solar luminosities in this band using the corresponding absolute magnitude of the Sun $K_\odot = 3.27$ (Willmer 2018). As we see, the X-ray luminosities of the AGNs vary in a wide range, from $L_X \sim 10^{41}$ to

$\sim 10^{45} \text{ erg s}^{-1}$, while their IR luminosities span a range of more than two orders of magnitude.

Figure 2 shows the distribution of the sample of galaxies from the combined 2MRS/2MPZ catalog in K -band luminosity and distance; the AGNs from the Swift/BAT sample are marked separately. As we see, the selected AGNs are, on average, slightly brighter in the infrared relative to the sample of all galaxies.

3.1 Allowance for the AGN Contribution to the IR Luminosity of Galaxies

Apart from the stellar population, the nucleus of an active galaxy can contribute noticeably to its K -band luminosity due to the absorption of part of the emission from the SMBH accretion disk by the surrounding dust and gas and its reradiation in the infrared. This contribution, $L_{K, \text{AGN}}$, can be estimated from the hard X-ray AGN luminosity using the correlation between these quantities. For the local AGN population this relationship was derived by Sazonov et al. (2012) based on data from the INTEGRAL sky survey in the 17–60 keV energy band and Spitzer Space Telescope observations and was converted to the K band by Khorunzhev et al. (2012). Adapting Eq. (4) from the latter paper for the Swift/BAT energy band (14–195 keV), we obtain

$$L_{K, \text{AGN}} \approx 0.05 L_X. \quad (1)$$

The conversion was made by assuming the X-ray AGN spectra to have a power-law shape with a slope $\Gamma = 1.8$ and an exponential cutoff at 200 keV (for a review, see Malizia et al. 2020). It should be emphasized that although the linear dependence (1) must describe satisfactorily the local AGN population on average, a significant

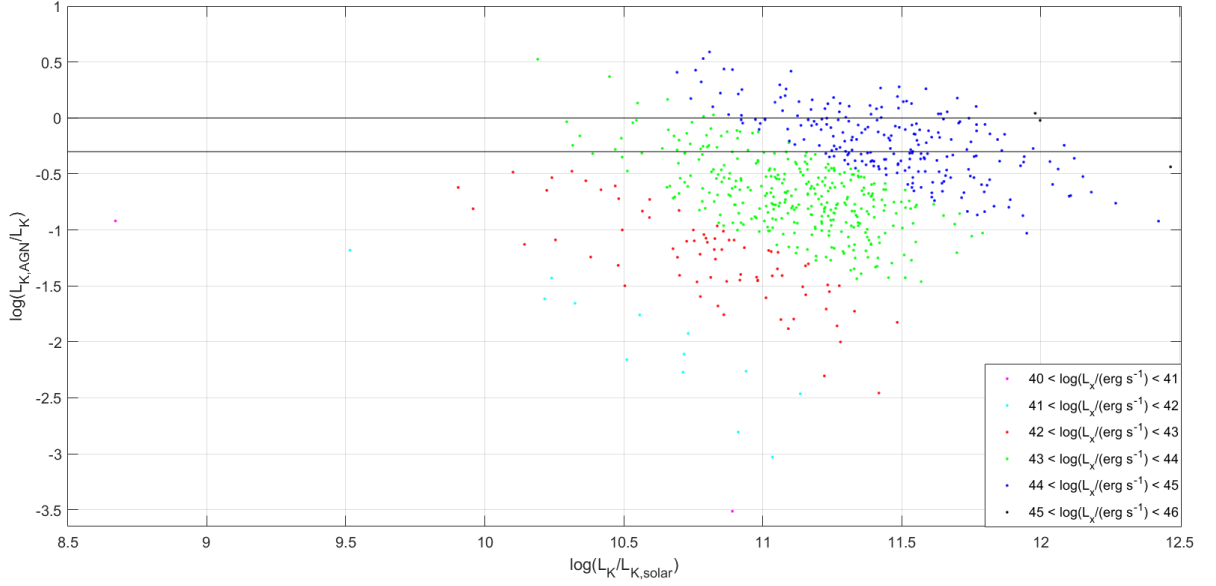


Figure 3. Ratio of the expected AGN contribution to the total galaxy luminosity in the K -band for the AGN sample (as a function of the luminosity). Different colors indicate objects with different hard X-ray luminosities. The two horizontal lines correspond to the 50 and 100% levels. Exceeding the 100% level corresponds to an overestimation of the AGN contribution.

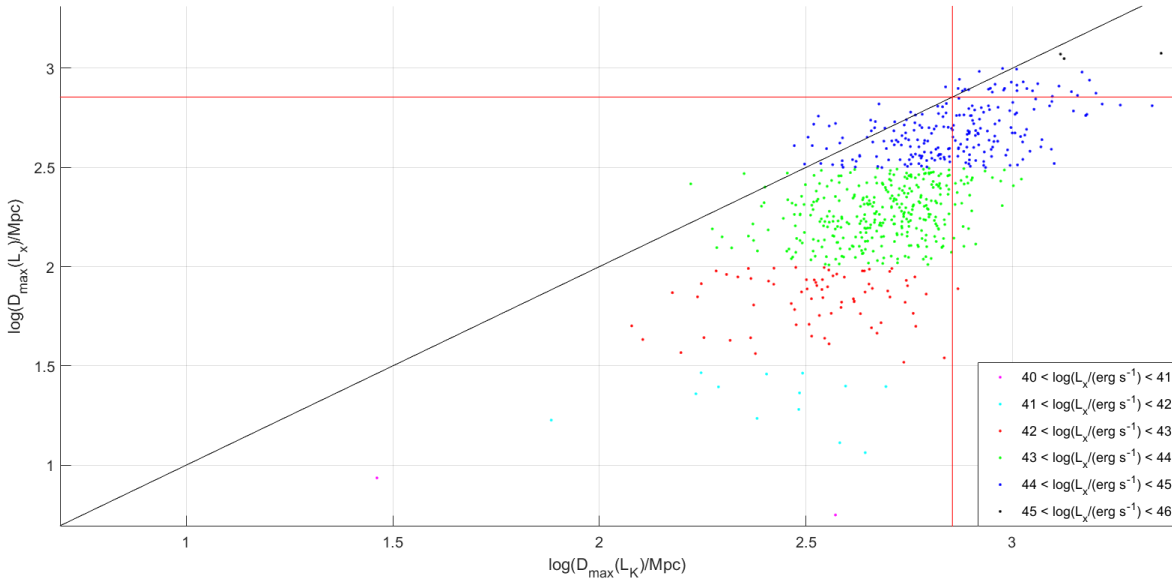


Figure 4. Maximum viewable distances in the Swift/BAT hard X-ray survey and the 2MASS K -band survey for AGNs of different luminosities (indicated by different colors) from the sample under study. The red lines mark the distances corresponding to $z = 0.15$.

scatter of $L_{K,AGN}/L_X$ from object to object is expected (Sazonov et al. 2012).

If we estimate the contribution of the nucleus to the IR luminosity of the AGNs from our sample in the described way, then the luminosities of their stellar populations can be estimated as

$$L_{K,g} = L_K - L_{K,AGN}. \quad (2)$$

Figure 3 shows the ratio $L_{K,AGN}/L_K$ for the AGN sample. For 169

objects the expected contribution of the nucleus to the total galaxy luminosity in the K band is more than 50%, while for 57 objects it exceeds 100%, suggesting an overestimation of the contribution of the nucleus for a number of objects. The related systematic uncertainty will be taken into account below when studying the λ_{Edd} distribution of SMBHs.

3.2 Luminosity Functions

Using the samples of objects described above, we can construct the luminosity functions of galaxies in the near infrared and of AGNs in hard X-rays at the present epoch ($z < 0.15$). The standard $1/V_{\max}$ method is suitable for such calculations, where $V_{\max} = (4\pi/3) \cdot 0.826 D_{\max}^3$ is the maximum volume of the Universe in which an object with a specified luminosity L_X or L_K could be detected in the corresponding survey (Swift/BAT or 2MASS). Here, the coefficient 0.826 is equal to the fraction of the total area of the celestial sphere at $|b| > 10^\circ$. We determined the maximum distance D_{\max} based on the Swift/BAT and 2MASS detection thresholds or, more specifically, the minimum flux of 8.4×10^{-12} erg s $^{-1}$ cm $^{-2}$ in the 14–195 keV band when constructing the X-ray AGN luminosity function and the maximum apparent magnitude $K = 13.9$ (Bilicki et al. 2013) when constructing the IR galaxy luminosity function. For the objects whose maximum viewable distance $D_{\max}(L_K)$ or $D_{\max}(L_X)$ exceeds $D_L(z = 0.15)$, V_{\max} was taken to be $(4\pi/3) \cdot 0.826 D_L^3(z = 0.15)$. We calculated the errors in the specified luminosity bins based on Poisson statistics as $\pm \sqrt{\sum_i (1/V_{\max,i}^2)}$.

Figure 4 shows the distribution of AGNs from the sample under study in maximum viewable distances in the Swift/BAT hard X-ray survey and the 2MASS K -band survey. We will need this two-dimensional distribution below when studying the λ_{Edd} distribution of SMBHs.

Apart from the discrete representation of the AGN and galaxy luminosity functions, we attempted to describe them by simple analytical models using the maximum likelihood method with the following likelihood function:

$$\mathcal{L} = -2 \sum_i \ln \frac{n(L_{\text{obs},i}) V_{\max}(L_{\text{obs},i})}{\int n(L_{\text{obs}}) V_{\max}(L_{\text{obs}}) d \log L_{\text{obs}}}, \quad (3)$$

where L_{obs} is the measured luminosity of the object in the corresponding survey. The summation over i is done over all of the objects from the corresponding sample, while the normalization of the likelihood function is determined by the total number of objects in the sample.

To describe the X-ray AGN luminosity function $n_X(L_X)$, we used a double power law:

$$n_X \equiv \frac{dN}{dV d \log L_X} = \frac{\phi^*}{(L_X/L^*)^{\gamma_1} + (L_X/L^*)^{\gamma_2}}, \quad (4)$$

which is commonly applied in AGN studies, while to describe the K -band galaxy luminosity function $n_K(L_K)$, we used a Schechter function:

$$n_K \equiv \frac{dN}{dV d \log L_K} = \phi^* \left(\frac{L_K}{L^*} \right)^{\alpha+1} \exp \left(-\frac{L_K}{L^*} \right). \quad (5)$$

3.2.1 Allowance for the AGN Sample Incompleteness

The sample of AGNs from the Swift/BAT survey being considered here is not statistically complete. First, there is a shortage of objects in 10% of the sky, because only 90% is covered with a sensitivity better than 8.4×10^{-12} erg s $^{-1}$ cm $^{-2}$. Second, in the original

Swift/BAT catalog there are 83 objects of an unknown nature at latitudes $|b| > 10^\circ$, and if we assume that half of them are AGNs, then our sample will increase by another $\sim 10\%$. This suggests that the sample under study is incomplete approximately by $20\% \pm 10\%$. Therefore, when constructing the AGN luminosity function and in all of the succeeding calculations, the AGN space density was multiplied by the coefficient 1.2, while the corresponding errors were increased by 10%.

3.2.2 X-ray AGN Luminosity Function

The hard X-ray AGN luminosity function calculated by the $1/V_{\max}$ method and its best fit by the model (4) are shown in Fig. (4), while the best-fit parameters are presented in Table 2.

As we see, the double power law model fits well the 105-month Swift/BAT survey data and agrees satisfactorily with the result obtained previously by Ajello et al. (2012) based on a smaller sample of AGNs from the 60-month Swift/BAT survey (for this comparison, we converted the model parameters given in Ajello et al. (2012) from the original 15–55 keV energy band to 14–195 keV using the model of a power-law spectrum with a slope $\Gamma = 1.8$ and an exponential cutoff at 200 keV).

3.2.3 K-band Galaxy Luminosity Function

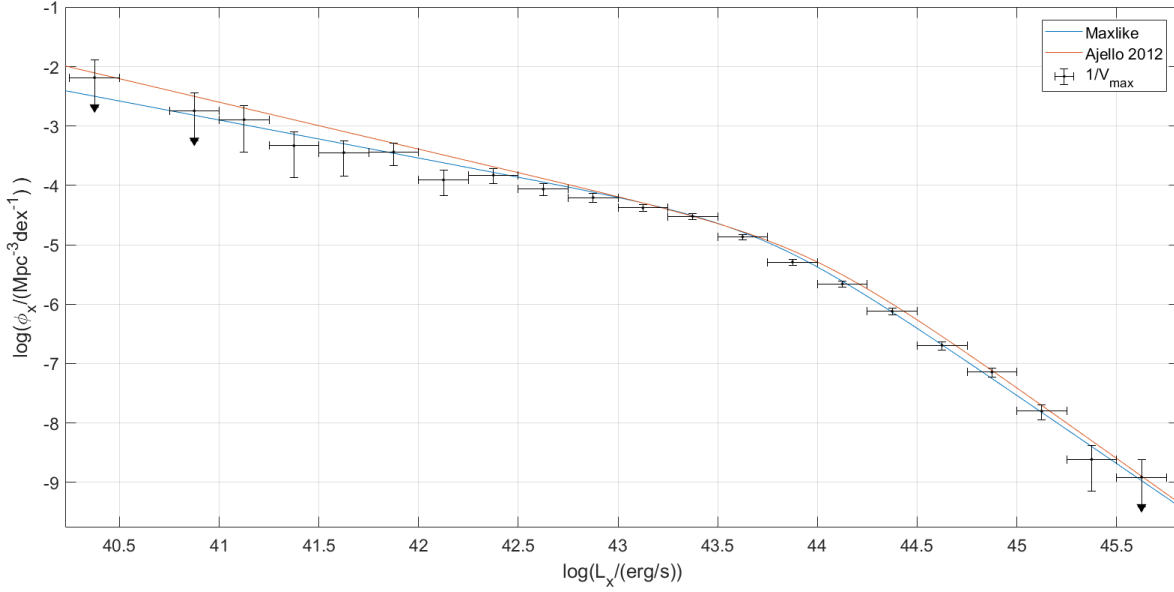
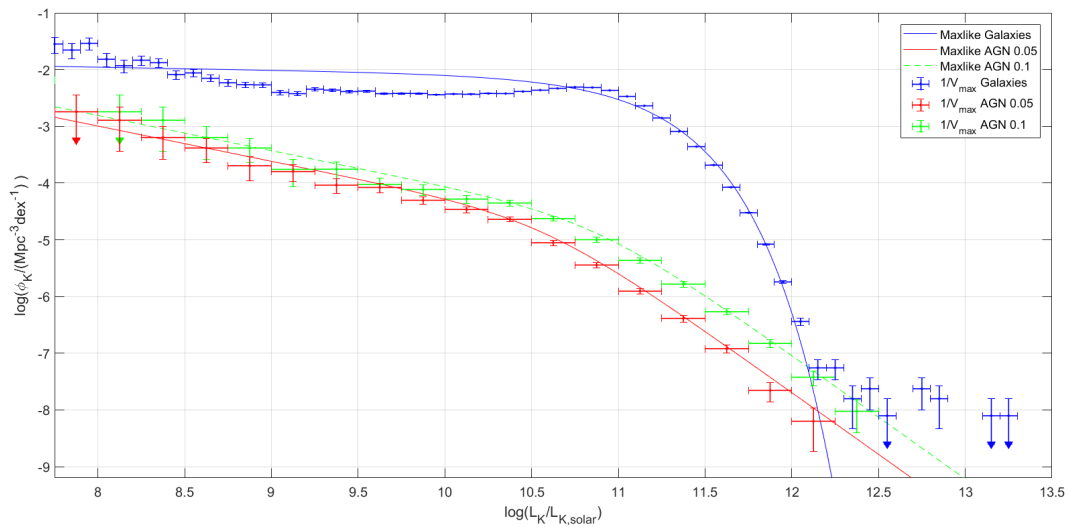
The K -band galaxy luminosity function calculated by the $1/V_{\max}$ method and its best fit by the model (5) are shown in Fig. 6, while the best-fit parameters are presented in Table 2.

Bonne et al. (2015) constructed the K -band galaxy luminosity function based on a sample of 13 325 nearby galaxies from the same 2MASS survey as that in our paper. Although the model parameters derived by us are close to those in Bonne et al. (2015) ($\phi^* = 7.64^{+0.93}_{-0.83} \times 10^{-3}$ Mpc $^{-3}$ dex $^{-1}$, $\alpha = -1.17 \pm 0.08$, $\log(L^*/\text{erg s}^{-1}) = 42.974 \pm 0.024$), it can be seen from Fig. 6 that the near-IR galaxy luminosity function is poorly described by the Schechter function. For low luminosities this is because our sample includes galaxies of both early (elliptical and lenticular) and late (spiral) types, and it would be more correct to describe the luminosity function by the sum of two Schechter models with different parameters (Bonne et al. 2015). In contrast, in the bright part of the luminosity function the observed deviation of the estimates by the $1/V_{\max}$ method from the analytical model probably stems from the fact that a noticeable fraction of the very-high-luminosity galaxies in 2MASS may be active, and the active nucleus (i.e., accretion onto the SMBH) can contribute noticeably to their K -band luminosity.

The correlation (1) can be used to estimate the AGN contribution to the bright part of the K -band galaxy luminosity function. For this purpose, we need to simply shift the hard X-ray AGN luminosity function (Fig. 5) found above (from the Swift/BAT data) by $|\log(0.05)|$ dex leftward along the luminosity axis. The AGN contribution to the K -band galaxy luminosity function estimated in this way is indicated by the red line in Fig. 6. We see that allowance for this contribution makes it possible to explain the observed bend of the galaxy luminosity function above $L_K \sim 10^{12.5} L_{K,\odot}$ only partially. This is most likely due to a significant uncertainty in the fraction of the bolometric AGN luminosity in the near infrared. For example, if we repeat the estimation by increasing the coefficient in

Table 2. Parameters of the best fit to the hard X-ray AGN luminosity function by the model (4) and the K -band galaxy luminosity function by the model (5)

Luminosity function	ϕ^* , $\text{Mpc}^{-3} \text{ dex}^{-1}$	γ_1 or α	γ_2	L^* , erg s^{-1}
AGNs	$2.2 \pm 0.2 \times 10^{-5}$	$0.64 \pm \begin{smallmatrix} 0.06 \\ 0.08 \end{smallmatrix}$	$2.28 \pm \begin{smallmatrix} 0.02 \\ 0.06 \end{smallmatrix}$	$5.623 \pm \begin{smallmatrix} 1.456 \\ 1.157 \end{smallmatrix} \times 10^{43}$
Galaxies	$7.89 \pm 0.01 \times 10^{-3}$	-1.053 ± 0.01		$6.79 \pm 0.02 \times 10^{42}$


Figure 5. The hard X-ray (14–195 keV) AGN luminosity function derived from the 105-month Swift/BAT survey data by the $1/V_{\text{max}}$ method (black dots with error bars). The blue line indicates the best fit by a double power law calculated by the maximum likelihood method. For comparison, the red line indicates the model from (Ajello et al. 2012) obtained from the 60-month Swift/BAT survey data.

Figure 6. The K -band galaxy luminosity function from the 2MASS data derived by the $1/V_{\text{max}}$ method (blue dots with error bars) and its best fit by the Schechter function calculated by the maximum likelihood method (blue line). Also shown are the K -band AGN luminosity functions derived by converting the corresponding hard X-ray luminosity function (Fig. 5) using the correlation (1) (red line) and a similar dependence, but with the coefficient 0.1 (green line).

Eq. (1) from 0.05 to 0.1, then it is possible to describe the bend of the galaxy luminosity function much better (see the green line in Fig. 6).

As follows from Fig. 6, up to $L_K \sim 10^{12.5} L_{K,\odot}$ the AGN contribution to the K -band galaxy luminosity function may be deemed negligible, i.e., at such luminosities the space density of ordinary (passive) galaxies is much higher than the AGN space density. Therefore, since there are no objects with $L_K > 10^{12.5} L_{K,\odot}$ in the AGN sample under study (from the Swift/BAT survey), in what follows we can not only restrict ourselves to $L_K < 10^{12.5} L_{K,\odot}$, but also assume that $n_K(L_{K,g}) \approx n_K(L_K)$ for the galaxy population (see Eq. (2)).

Despite the fact that the simple Schechter model describes poorly the K -band galaxy luminosity function, this in no way affects the results of our study, because below we use only the nonparametric description of this function (the discrete estimates of the galaxy space density obtained by the $1/V_{\max}$ method).

4 EDDINGTON RATIO DISTRIBUTION OF AGNS

We now turn to the direct goal of our paper – the study of the Eddington ratio distribution of SMBHs and its dependence of the galaxy mass.

4.1 Mass-to-Light Ratio and Galaxy Stellar Mass Function

First of all we need to pass from the near-IR luminosity to the galaxy stellar mass. The mass-to-light ratio is known to depend on the galaxy type. For example, for spiral galaxies McGaugh and Schombert (2014) obtained a typical value of $M_*/L_K = 0.6 M_\odot/L_{K,\odot}$, while Martinsson et al. (2013) provided the range of $M_*/L_K = (0.31 \pm 0.07) M_\odot/L_{K,\odot}$. In Bell et al. (2003) Fig. 20 presents the B - R color- M_*/L_K correlation for galaxies from 2MASS (i.e., galaxies of different types were included). This correlation is weak: for most galaxies $0.5 M_\odot/L_{K,\odot} < M_*/L_K < 1.2 M_\odot/L_{K,\odot}$, while the mean is $\approx 0.8 M_\odot/L_{K,\odot}$. Based on these observational data, below we will use a constant value,

$$\frac{M_*}{L_{K,g}} = 0.6 \frac{M_\odot}{L_{K,\odot}}, \quad (6)$$

understanding that this ratio can actually vary by $\sim 50\%$ for galaxies from the sample under study.

Under this assumption we can pass from the K -band galaxy luminosity function $n_K(L_{K,g}) \approx n_K(L_K)$ to the galaxy stellar mass function $n_m(M_*)$ by shifting the argument of the function by $\log(0.6)$.

4.2 Eddington Ratio

It is convenient to describe the intensity of accretion onto SMBHs in terms of the ratio of the bolometric luminosity to the Eddington limit (Eddington ratio):

$$\lambda_{\text{Edd}} \equiv \frac{L_{\text{bol}}}{L_{\text{Edd}}}, \quad (7)$$

where

$$L_{\text{Edd}} = 1.3 \cdot 10^{38} \frac{M_{\text{BH}}}{M_\odot} \quad (8)$$

(erg s^{-1}), and M_{BH} is the BH mass.

Based on a sample of AGNs (in the local Universe) from the INTEGRAL hard X-ray survey, Sazonov et al. (2012) showed that the luminosity of AGNs in the 17–60 keV energy band is, on average, about 1/9 of their bolometric luminosity. Assuming (as we have already done above) that the X-ray spectra of AGNs are described by a power law with a slope $\Gamma = 1.8$ and an exponential cutoff at 200 keV, we can write a similar relation to estimate the bolometric AGN luminosity from the measured luminosity in the Swift/BAT energy band (14–195 keV):

$$L_{\text{bol}} \approx 4.5 L_X. \quad (9)$$

4.3 Calculating the λ_{Edd} Distribution of Galaxies

Our goal is to determine the probability $f(\lambda_{\text{Edd}}|M_*)$ that the SMBH in the nucleus of a galaxy with a stellar mass M_* accretes matter at a rate λ_{Edd} . This quantity can be found as follows:

$$f(\lambda_{\text{Edd}}|M_*) = \frac{n_{ml}(M_*, \lambda_{\text{Edd}})}{n_m(M_*)}, \quad (10)$$

where

$$n_{ml}(M_*, \lambda_{\text{Edd}}) \equiv \frac{dN_{\text{gal}}/dV}{d \log \lambda_{\text{Edd}} d \log M_*} \quad (11)$$

is the galaxy space density per unit logarithmic interval of λ_{Edd} and unit logarithmic interval of M_* near the specified λ_{Edd} and M_* , respectively.

We calculated $n_{ml}(M_*, \lambda_{\text{Edd}})$ by the $1/V_{\max}$ method, where V_{\max} is the smaller of the volumes $V_{\max}(L_{K,g})$ and $V_{\max}(L_X)$ for a given AGN. The applicability of this method and related uncertainties are discussed below. It can be seen from Fig. 4 that for the AGNs of the sample under study the maximum viewable volume V_{\max} is determined mainly by the sensitivity of the Swift/BAT X-ray survey rather than the IR 2MASS survey.

4.3.1 Allowance for the Uncertainty in Estimating the Stellar Masses of Galaxies with Active Nuclei

The calculation of $n_{ml}(M_*, \lambda_{\text{Edd}})$ consists of several steps:

i For each AGN (out of the 653) we estimate the K -band galaxy stellar luminosity $L_{K,g}$ from Eq. (2) by taking into account the expected contribution of the active nucleus to the galaxy luminosity using Eq. (1) and then the stellar mass M_* from Eq. (6). In this step $L_{K,g} < 0$ is obtained for some objects and, naturally, these are excluded from further consideration.

ii For each of the remaining AGNs we calculate $D_{\max}(L_{K,g})$, i.e., the maximum distance to which this object would be detected in 2MASS if it had no active nucleus. If, as a result, $D_{\max}(L_{K,g})$ turns out to be smaller than the distance D to the object, then this AGN is excluded from further consideration.

iii For each of the objects selected in the preceding steps we determine the maximum viewable volume $V_{\max}(L_{K,g}, L_X) = \min(V_{\max}(L_X), V_{\max}(L_{K,g}))$.

Thus, we got three groups of AGNs:

- (1) 536 objects with $D < D_{\max}(L_{K,g})$ and $L_{K,g} > 0$,
- (2) 60 objects with $D > D_{\max}(L_{K,g})$ and $L_{K,g} > 0$,
- (3) 57 objects with $L_{K,g} \leq 0$.

The presence of objects with $L_{K,g} \leq 0$ suggests that we overestimated the contribution of the active nucleus to the K -band luminosity of these galaxies. Previously (Fig. 3) we have already noted that the $L_{K,AGN}$ estimates are characterized by a significant uncertainty. To take into account the influence of this factor on the results of our study, we calculated $n_{ml}(M_*, \lambda_{Edd})$ by three methods.

The first method is based on the algorithm described above. Specifically, we take into account the contribution of the active nucleus to the IR galaxy luminosity based on Eq. (1) and use the subsample of 536 AGNs with $D < D_{\max}(L_{K,g})$ and $L_{K,g} > 0$ in our calculation. In this case, the AGN stellar masses, on average, are somewhat underestimated.

We also performed an alternative calculation of $n_{ml}(M_*, \lambda_{Edd})$ by completely neglecting the contribution of the active nucleus when calculating the galaxy masses, i.e., by assuming $L_{K,g} = L_K$. In this case, the total sample of 653 AGNs is used in our calculation, but the galaxy stellar masses are overestimated.

Finally, we performed a calculation by the third method, which is a modification of the first one. Specifically, for all of the objects with $L_{K,g} \leq 0$ the K -band galaxy luminosity was estimated as $L_{K,g}^* = 0.5L_K$ (in the remaining cases, as above, $L_{K,g}^* = L_K - L_{K,AGN}$). In this case, the final sample for calculating $n_{ml}(M_*, \lambda_{Edd})$ was 556 objects (for the remaining 97 $D > D_{\max}(L_{K,g}^*)$).

The third method may be deemed intermediate between the first and second ones, which probably give extreme estimates of $n_{ml}(M_*, \lambda_{Edd})$. The errors of $n_{ml}(M_*, \lambda_{Edd})$ in each specified interval of M_* and λ_{Edd} were calculated as $\Delta_{\text{tot}} = \sqrt{\Delta_{\text{stat}}^2 + \Delta_{\text{syst}}^2}$. We estimated the statistical error Δ_{stat} as $\sqrt{\sum 1/V_{\max}^2}$ and the systematic one (the error of the method) Δ_{syst} as the difference between the extreme estimates obtained by the first and second methods of estimating the AGN contribution described above. The final error of $f(\lambda_{Edd}|M_*)$ was calculated according to the definition (10), as $\Delta f \approx \Delta n_{ml}/n_m + \Delta n_m \frac{n_{ml}}{n_m^2}$, i.e., the error of the galaxy stellar mass function $n_m(M_*)$ was deemed negligible.

4.3.2 Estimating the SMBH Masses

Despite the fact that the sample of AGNs from the Swift/BAT survey used in this paper consists of relatively nearby objects ($z < 0.15$) and has been studied reasonably well, the estimates of the BH masses in these objects are characterized by a significant uncertainty. To estimate the influence of this factor on the results of our study, we used two types of M_{BH} estimates for the AGN sample.

First, for all AGNs M_{BH} were estimated from the known correlation of the SMBH mass with the K -band stellar bulge luminosity

$L_{K,b}$ (i.e., basically, from the correlation with the bulge mass (Kormendy and Ho 2013)):

$$\frac{M_{BH}}{10^9 M_{\odot}} = 0.544 \left(\frac{L_{K,b}}{10^{11} L_{K,\odot}} \right)^{1.22}. \quad (12)$$

The bulge luminosity was estimated as $L_{K,b} = P_b L_{K,g}$, where P_b is the fraction of the bulge in the total stellar mass of the galaxy. The latter depends on the morphological type of the galaxy. It should also be kept in mind that relation (12) was derived for galaxies with classical bulges, while its application in the case of galaxies with pseudo-bulges can lead to a significant error in estimating the BH masses (Kormendy and Ho 2013). Because of the lack of information about the morphology of the objects under study, we fixed P_b at 0.25 for all of the AGNs from the Swift/BAT survey. Note that $P_b = 1$ for elliptical galaxies, $P_b \approx 0.25$ – 0.2 for S0–Sb galaxies, and $P_b \approx 0.08$ for Sc galaxies (see, e.g., Laurikainen et al. 2007, 2010; Graham and Worley 2008). Below the estimates based on Eq. (12) are called “rough estimates.”

Second, for AGNs we used the M_{BH} estimates obtained by more accurate methods from Koss et al. (2017) and Marchesini et al. (2019) (see Table 3). Such estimates (hereafter “accurate estimates”) exist approximately for half of the AGN sample under study or, more specifically, for 332 of the 653 objects. If several different M_{BH} estimates were available, then we preferred those obtained by the reverberation mapping method and, subsequently, in order of priority: the estimates from the width and luminosity of the broad $H\alpha$ emission line, from the width of the $H\beta$ emission line and the optical continuum luminosity, and from the correlation of the SMBH mass with the stellar velocity dispersion in galaxies.

Figure 7 (top left) shows the hard X-ray luminosity distribution of the AGNs for which only rough SMBH mass estimates are available and those for which accurate estimates are available. As we see, the fraction of AGNs with accurate estimates in the sample under study is virtually independent of L_X . The same figure (bottom left) shows the distribution of rough and accurate M_{BH} estimates. The second distribution is seen to be wider (for example, judging by the full width at half maximum of the distribution) than the first one.

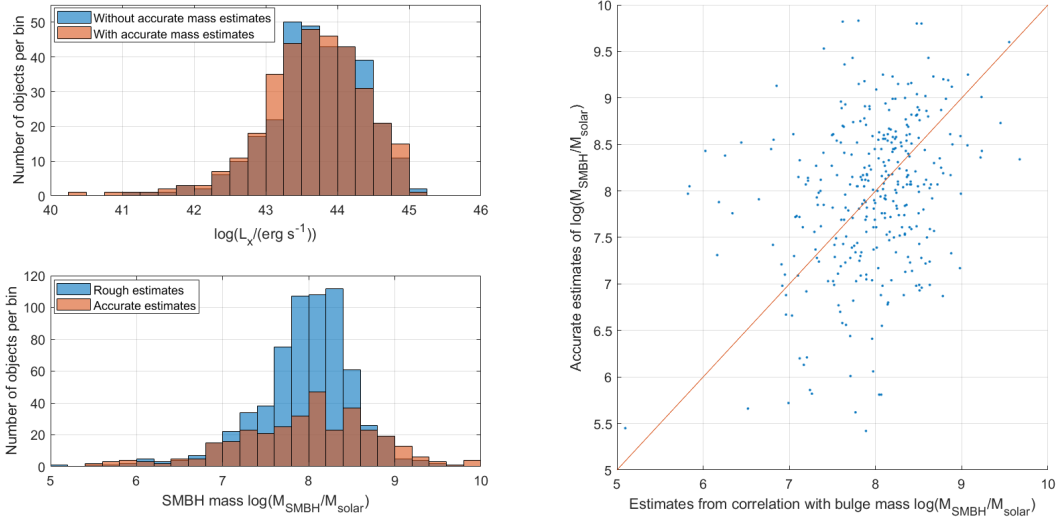
The existing uncertainty in the SMBH mass estimates for the AGN sample is best demonstrated by the diagram presented on the right in Fig. 7, where the rough and accurate M_{BH} estimates for the subsample of 332 AGNs are compared directly. There is a large scatter: the rms deviation between the logarithms of the rough and accurate estimates is 0.86 dex.

To take into account the influence of the uncertainty in the SMBH mass estimates in AGNs on the results of our study, we calculated $n_{ml}(M_*, \lambda_{Edd})$ by three methods (in addition to the three different methods of allowance for the active nucleus described in the previous subsection when calculating the stellar mass).

The first method consists in using the rough M_{BH} estimates for the entire AGN sample (653 objects). The second one consists in using only the accurate estimates for the subsample of 332 objects. The previously noted fact (Fig. 7) that the fraction of the AGNs in the sample under study for which there are accurate SMBH mass estimates is virtually independent of the X-ray luminosity, i.e., no noticeable selection effect with regard to this characteristic is observed, serves as a basis for the applicability of this approach.

Table 3. The number of AGNs with “accurate” SMBH mass estimates obtained by different methods

Reverberation mapping	From H α	From H β	From velocity dispersion	Total
39	179	149	164	332

**Figure 7.** Top left: Hard X-ray luminosity (L_X) distribution of the AGNs for which only the SMBH mass estimate from the K -band galaxy luminosity (“rough estimate”) is available (321 of the 653 objects) and those for which more accurate SMBH mass estimates are available (332 of the 653 objects). The bin width is 0.25 order of magnitude. Bottom left: The M_{BH} distribution of rough SMBH mass estimates for all of the sample AGNs and more accurate estimates for the subsample of 332 objects. The bin width is 0.2 order of magnitude. Right: Comparison of the rough and accurate M_{BH} estimates for the subsample of 332 AGNs.

In this case, however, the incompleteness coefficient $\kappa = 653/332$ is required to be introduced when calculating n_{ml} :

$$n_{ml}(M_*, \lambda_{\text{Edd}}) = \kappa \sum_i \frac{1}{V_{\text{max},i}}. \quad (13)$$

The summation in Eq. (13) is over all of the AGNs in a given interval in M_* and $\log \lambda_{\text{Edd}}$. Accordingly, the statistical errors are calculated as $\pm \sqrt{\kappa \sum 1/V_{\text{max},i}^2}$.

The third method (“mixed estimates”) is based on the accurate M_{BH} estimates for the subsample of 332 AGNs and the rough estimates for the remaining 321 sample objects.

As regards the applicability of the $1/V_{\text{max}}$, the volume in which all of the AGNs with specified $L_{K,g}$ (or, identically, $L_{K,g}^*$) and λ_{Edd} can be detected should be used as V_{max} in the first method of estimating the SMBH masses. Since the X-ray luminosity L_X is uniquely determined via $L_{K,g}$ and λ_{Edd} in the rough SMBH estimate, this is equivalent to the volume in which all of the AGNs with given $L_{K,g}$ and L_X can be detected. For the second method the viewable volume for each AGN with an accurate M_{BH} may be deemed to be the same as that in the first method, but (supposing that in this volume λ_{Edd} for the AGNs without accurate M_{BH} are distributed in the same way as those for the objects with accurate M_{BH} estimates, based on the top left histogram in Fig. 7) then we should assume that it contains a factor of κ more objects. The third

method supposes to take the viewable volume to be the same as that in the first method. Here, there is no need to make a correction for incompleteness, because the incompleteness of the objects with accurate estimates in a specific volume is compensated for by the objects with rough estimates.

5 RESULTS

Figure 8 shows the calculated dependence $f(\lambda_{\text{Edd}}|M_*)$ in six galaxy stellar mass intervals of width 0.5 dex from $\log(M_*/M_{\odot}) = 9.28$ to 12.28. This range is determined by the boundaries of the K -band luminosity range for the AGNs of the sample under study ($8.5 < \log(L_K/L_{K,\odot}) < 12.5$, see, e.g., Fig. 1) and the $L_{K,g}$ - to- M_* conversion factor in Eq. (6), but we additionally limited the luminosity range from below by $\log(L_{K,g}/L_{K,\odot}) = 9.5$, because below this value there is only one AGN in our sample. Different colors in the figure indicate the dependences derived by using the two extreme methods of allowance for the active nucleus in calculating the galaxy stellar mass: the first (when M_* is estimated from $L_{K,g}$) and the second (when the total galaxy luminosity L_K is used instead of $L_{K,g}$). In this case, to calculate λ_{Edd} , we used the mixed M_{BH} estimates (third method).

In most of the $\log M_*$ intervals $f(\lambda_{\text{Edd}})$ clearly shows a falling trend, with the uncertainty due to the influence of the active nucleus

Table 4. The best fits to the dependence $f(\lambda_{\text{Edd}}|M_*)$ by a power law in λ_{Edd} with M_* -independent parameters (Eq. (14)) for different SMBH mass estimates. The most probable values of the parameters and (in parentheses) the 1σ confidence intervals are given

Best-fit parameter	From rough estimates	From accurate estimates	From mixed estimates
Normalization $\log(A/\text{dex}^{-1})$	-5.07 (-5.19, -4.95)	-3.55 (-3.66, -3.45)	-3.79 (-3.93, -3.68)
Slope γ	-1.3 (-1.36, -1.24)	-0.71 (-0.77, -0.65)	-0.82 (-0.91, -0.76)
χ^2 at minimum	35.78	28.1	15
Number of degrees of freedom $n - k$	24	14	18
AIC_c	40.3	33.02	19.7
BIC	42.29	33.65	20.99

Table 5. The best fits to the dependence $f(\lambda_{\text{Edd}}|M_*)$ by a Schechter function in λ_{Edd} with M_* -independent parameters (Eq. (15)) for different SMBH mass estimates

Best-fit parameters	From rough estimates	From accurate estimates	From mixed estimates
Normalization $\log(A/\text{dex}^{-1})$	-2.13 (-2.35, -1.96)	-3.07 (-3.35, -2.85)	-3.72 (-4.28, -3.35)
Slope γ	-0.56 (-0.72, -0.39)	-0.44 (-0.54, -0.33)	-0.67 (-0.79, -0.55)
$\log \lambda_{\text{Edd}}^*$	-1.68 (-1.77, -1.58)	0.16 (-0.04, 0.34)	0.35 (0.02, 0.8)
χ^2 at minimum	17.3	18.65	12.34
Number of degrees of freedom $n - k$	23	13	17
AIC_c	24.39	26.65	19.84
BIC	27.07	26.96	21.33

Table 6. The best fits to the dependence $f(\lambda_{\text{Edd}}|M_*)$ by a power law in M_* and by a Schechter function in λ_{Edd} (Eq. (16)), for different SMBH mass estimates

Best-fit parameters	From rough estimates	From accurate estimates	From mixed estimates
Normalization $\log(B/\text{dex}^{-1})$	-2.34 (-2.82, -2.02)	-3.53 (-4.34, -2.36)	-3.89 (-5.36, -3.26)
Slope θ	-0.24 (-0.38, -0.1)	-0.33 (-0.51, -0.08)	-0.11 (-0.26, 0.05)
Slope γ	-0.7 (-0.95, -0.46)	-0.6 (-0.74, -0.45)	-0.71 (-0.88, -0.54)
$\log \lambda_{\text{Edd}}^*$	-1.61 (-1.76, -0.37)	0.35 (-0.2, 1.04)	0.43 (-0.16, 1.8)
χ^2 at minimum	11.17	15.15	11.37
Number of degrees of freedom $n - k$	22	12	16
AIC_c	21.08	26.78	22.04
BIC	24.2	26.24	23.36

on the K -band galaxy luminosity having no strong influence on the shape of the dependence.

Figure 9 shows the analogous dependences derived by the intermediate method of allowance for the active nucleus when calculating the galaxy stellar mass (using $L_{K,g}^*$) and three different methods of estimating the SMBH masses or, more specifically, based on the rough, accurate, and mixed M_{BH} estimates. We see a significant scatter of values due to the uncertainty in the M_{BH} estimates for the AGN sample under study.

Given that the dependence $f(\lambda_{\text{Edd}})$ falls off, we attempted to describe it by a power law with a slope and normalization independent of the stellar mass:

$$f(\lambda_{\text{Edd}}|M_*) = A\lambda_{\text{Edd}}^\gamma. \quad (14)$$

It was fitted using the χ^2 test based on the data points estimated by the $1/V_{\text{max}}$ method, given the corresponding errors. The calculation was performed by the intermediate method of allowance for the contribution of the active nucleus to the IR galaxy luminosity and by taking into account the related statistical uncertainty (as was described in the Subsection “Allowance for the Uncertainty in Estimating the Stellar Masses of Galaxies with Active Nuclei”).

Here and below, we decided to use only the range $\log \lambda_{\text{Edd}} > -3$ because the power-law trend is expected to be smoothed out at lower Eddington ratios, as, for example, noted in Georgakakis et al. (2014) and Aird et al. (2018) for the earlier Universe, or even exhibits a break. In the dependences derived by us (see Figs. 8 and 9) this trend is also visible in the M_* intervals where there are data points with $\log \lambda_{\text{Edd}} < -3$, i.e., $10.28 < \log(M_*/M_\odot) < 10.78$ and $10.78 < \log(M_*/M_\odot) < 11.28$. However, based on the available

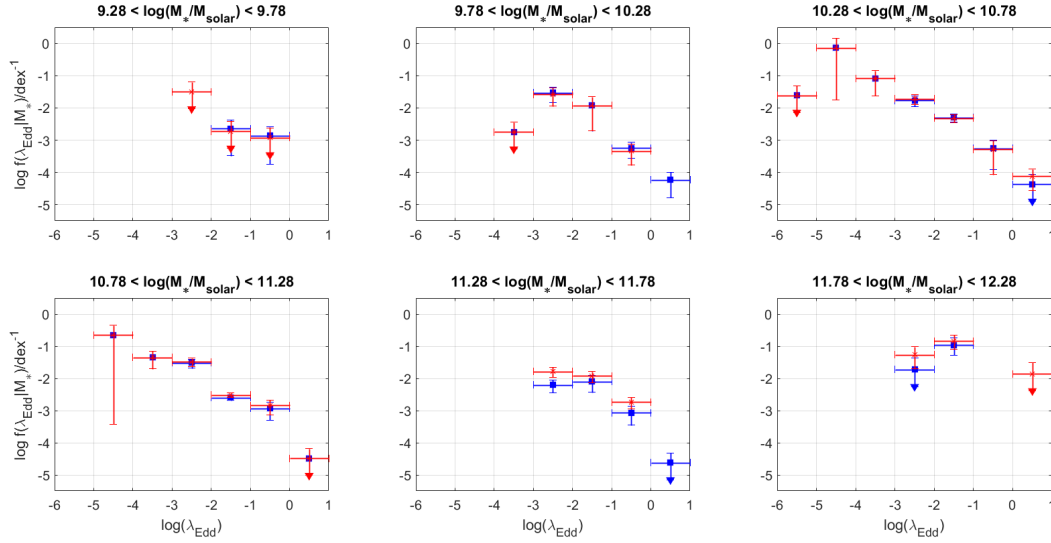


Figure 8. The dependence $f(\lambda_{\text{Edd}})$ for different intervals of the galaxy stellar mass M_* , calculated by the $1/V_{\text{max}}$ method. The results obtained by using the two extreme methods of allowance for the active nucleus in calculating M_* are compared: the first (based on $L_{K,g}$, blue dots) and the second (based on L_K , red dots). In both cases, we used mixed (rough and accurate) SMBH mass estimates.

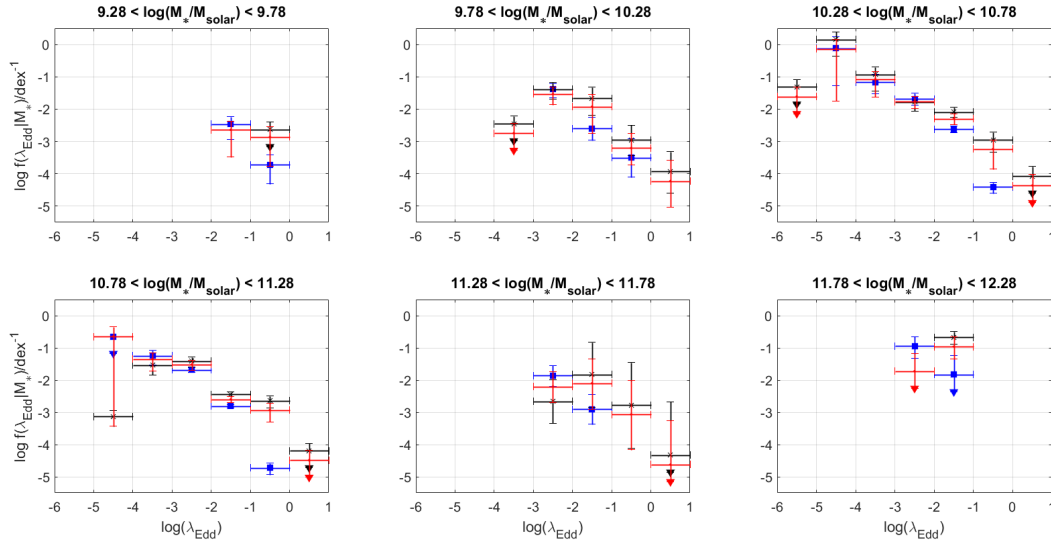


Figure 9. Same as (Fig. 8), but for different types of SMBH mass estimates: the rough (blue), accurate (black), and mixed (red) ones. The intermediate method of allowance for the active nucleus (using $L_{K,g}^*$, see the text) was used everywhere in calculating the stellar mass.

data, it is hard to say something more specific about the pattern of the dependence $f(\lambda_{\text{Edd}})$ at $\log \lambda_{\text{Edd}} < -3$. It will be interesting to study this question in future based on larger AGN samples.

The fitting was performed separately for three variants of the dependence $f(\lambda_{\text{Edd}})$: based on the rough, accurate, and mixed M_{BH} estimates; we used 0.5 dex and 1 dex λ_{Edd} bins in the first case and the two remaining ones, respectively. The results of our modeling are shown in Figs. 10 and 11, while the corresponding parameters of the power-law dependence are given in Table 4.

As can be seen from the table and the graphs, the single power-law model describes well the dependence $f(\lambda_{\text{Edd}})$ derived from the mixed M_{BH} estimates, but much more poorly the dependences

calculated from the rough or accurate estimates. At the same time, the derived parameters also vary significantly

In the next step we attempted to add an exponential cutoff at large λ_{Edd} to the power-law dependence on λ_{Edd} , i.e., to describe the data by an analog of the Schechter function:

$$f(\lambda_{\text{Edd}} | M_*) = A \left(\frac{\lambda_{\text{Edd}}}{\lambda_{\text{Edd}}^*} \right)^\gamma \exp \left(- \frac{\lambda_{\text{Edd}}}{\lambda_{\text{Edd}}^*} \right), \quad (15)$$

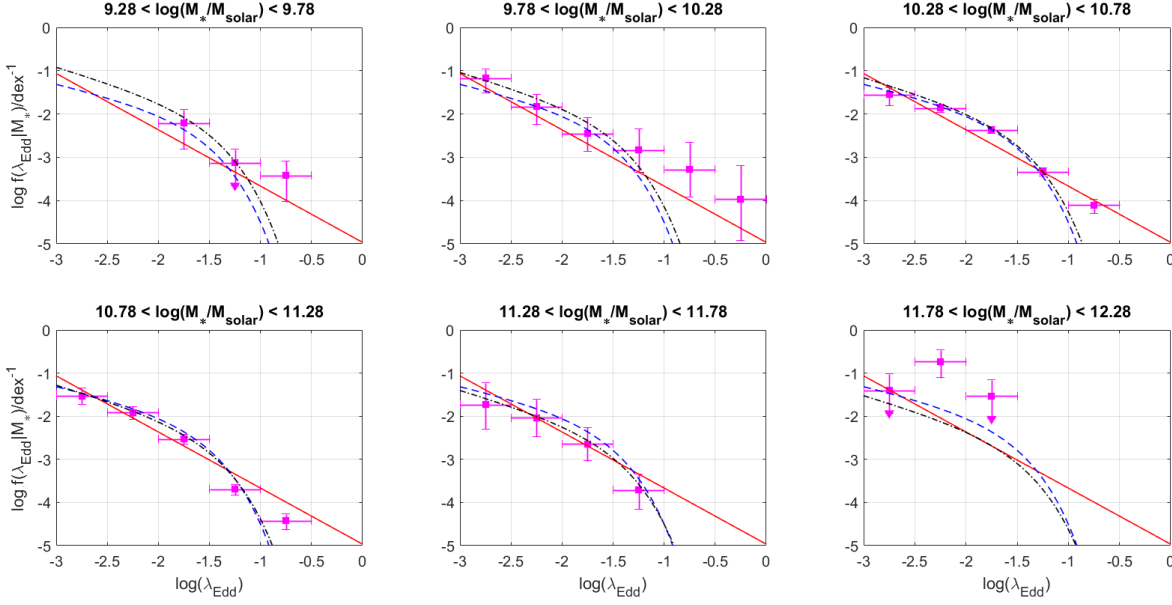


Figure 10. The dependence $f(\lambda_{\text{Edd}})$ calculated by the $1/V_{\text{max}}$ method using the rough M_{BH} estimates and its best fit by different models: a power law with single (M_* -independent) parameters (red solid line), a Schechter function in λ_{Edd} with single parameters (blue dashed line), and a Schechter function in λ_{Edd} with a power-law dependence of the normalization on M_* (black dotted line).

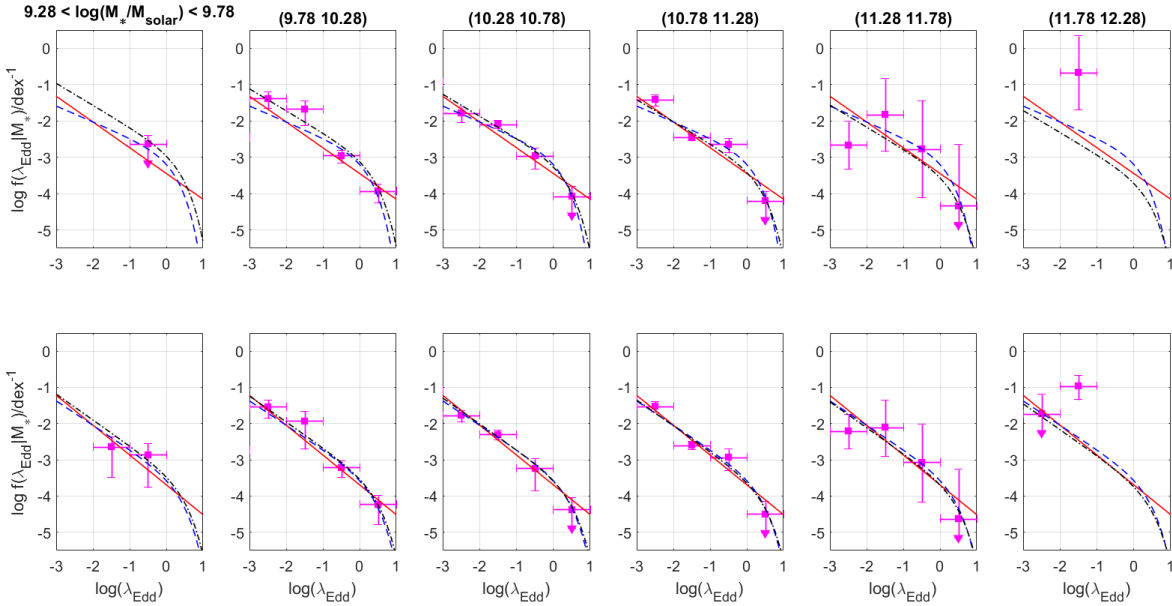


Figure 11. Same as Fig. 10, but when using the accurate (the upper row of graphs) and mixed (the lower row of graphs) M_{BH} estimates.

and then also a power-law dependence on the stellar mass:

$$f(\lambda_{\text{Edd}}|M_*) = B \left(\frac{M}{M'} \right)^\theta \left(\frac{\lambda_{\text{Edd}}}{\lambda_{\text{Edd}}^*} \right)^\gamma \exp \left(-\frac{\lambda_{\text{Edd}}}{\lambda_{\text{Edd}}^*} \right), \quad (16)$$

where $M' = 10^{11} M_\odot$. The best fits by these models are shown in the same Figs. 10 and 11, while the corresponding parameters are given in Tables 5 and 6.

To compare the models, we used a corrected Akaike information criterion for the χ^2 distribution:

$$AIC_c = 2k + \chi^2 + \frac{2k(k+1)}{n-k-1}, \quad (17)$$

where k is the number of model parameters, n is the number of data points, and χ^2 is the χ^2 value of the model. The smaller the value of AIC_c , the better the model. The derived AIC_c for all of the models used are given in the next-to-last rows of Tables 4–6.

Based on these values, we can conclude that adding an exponential cutoff to the power-law dependence on λ_{Edd} improves the quality of the fit when using the rough M_{BH} estimates. For the accurate M_{BH} estimates the improvement is less significant, while for the mixed ones introducing a new parameter does not lead to any improvement. Adding a powerlaw dependence on the galaxy stellar mass slightly improves the quality of the fit for the rough M_{BH} estimates, but does not lead to any improvements for the accurate and mixed M_{BH} estimates.

The Bayesian information criterion $BIC = k \ln n + \chi^2$ yields similar results (the lower rows in Tables 4–6), except for the insignificant improvement of the fit for the accurate M_{BH} estimates when introducing a power-law dependence on M_* .

Significant errors in the parameters γ and λ_{Edd}^* when fitting the dependences $f(\lambda_{\text{Edd}})$ by a Schechter function, especially for the model (16), can also be noted. The slope θ for this model applied to the mixed M_{BH} estimates is consistent with zero; for the other samples (the rough and accurate M_{BH} estimates) the dependence on the stellar mass is also weak.

To summarize the results obtained, it can be noted that adding an exponential cutoff to the power-law dependence on λ_{Edd} improves significantly the quality of the fit only when using the rough M_{BH} estimates, with the slope of the dependence (below the cutoff) in this case being in good agreement with the slope of $f(\lambda_{\text{Edd}})$ for the accurate or mixed M_{BH} estimates (for all models). Thus, the slope of $f(\lambda_{\text{Edd}})$ may be deemed to have been reliably measured in the interval of $\log \lambda_{\text{Edd}}$ from -3 to -1.5 : $\gamma = -0.7 \pm 0.15$. At the same time, the position of the cutoff at $\lambda_{\text{Edd}} \sim 1$ (near the critical accretion rate) cannot yet be deemed to have been reliably found due to the existence of significant systematic uncertainties (associated mainly with the SMBH mass estimate).

The slope of $f(\lambda_{\text{Edd}})$ measured in this paper for the local Universe is consistent, given the errors, with the estimate obtained previously by Aird et al. (2012) for the Universe at $0.2 < z < 1$: $\gamma = -0.65 \pm 0.04$. In addition, the normalization of the power-law dependence $f(\lambda_{\text{Edd}}) \log A = -3.79$ (-3.93 , -3.68) dex derived here also agrees with the normalization from the mentioned paper $\log A_{z=0} = -3.86 \pm 0.1$ dex, given the correction for evolution based on the formula $A_z = A_{z=0.6} ((1+z)/(1+0.6))^{3.47 \pm 0.5}$, where $\log A_{z=0.6} = -3.15 \pm 0.08$ dex, from the same paper.

5.1 Mean Growth Time and Duty Cycle of SMBHs at the Present Epoch

The derived dependence $f(\lambda_{\text{Edd}})$ characterizes the distribution of current mass accretion rates onto SMBHs in the local Universe ($z < 0.15$), being basically a “snapshot” of the process of accretion onto the BHs in galactic nuclei. From this dependence we can infer the mean SMBH growth time at the present epoch. Indeed, although the growth histories of different BHs could differ greatly from one another, as a first approximation, we can assume that the distribution of instantaneous accretion rates (λ_{Edd}) for a specific BH on a long time scale ($\sim 1\text{--}2$ Gyr, i.e., the time interval between $z = 0.15$ and $z = 0$ being studied in this paper) roughly corresponds to the present-day distribution $f(\lambda_{\text{Edd}})$ for the population of SMBHs as a whole.

Let us define the characteristic BH growth time τ as

$$\int_0^\tau \frac{\dot{M}_{\text{BH}}}{M_{\text{BH}}} dt = 1, \quad (18)$$

where

$$\frac{\dot{M}_{\text{BH}}}{M_{\text{BH}}} = \frac{L_{\text{bol}}}{\eta c^2 M_{\text{BH}}} = 7.3 \times 10^{-16} \lambda_{\text{Edd}} \quad (19)$$

(s^{-1}), $\eta = 0.1$ is the expected accretion efficiency onto SMBHs, and c is the speed of light in a vacuum. Here, we used relations (7) and (8).

By introducing the definition of the mean accretion rate in units of the Eddington ratio,

$$\langle \lambda_{\text{Edd}} \rangle \equiv \frac{1}{\tau} \int_0^\tau \lambda_{\text{Edd}} dt, \quad (20)$$

we get

$$\tau = 4.4 \times 10^7 \langle \lambda_{\text{Edd}} \rangle^{-1} \quad (21)$$

(years), where instead of the time averaging we can use (in accordance with the above assumption) the averaging over the present-day population of SMBHs:

$$\langle \lambda_{\text{Edd}} \rangle = \int_{-\infty}^{+\infty} f(\lambda_{\text{Edd}}) \lambda_{\text{Edd}} d \log \lambda_{\text{Edd}}. \quad (22)$$

We calculated τ from the discrete dependences $f(\lambda_{\text{Edd}})$ presented in Fig. 9 in separate galaxy stellar mass intervals using, as above, different types of SMBH mass estimates (rough, accurate, and mixed). The quantity $\langle \lambda_{\text{Edd}} \rangle$ was calculated by summing over the λ_{Edd} intervals, i.e., $\sum_i f(\lambda_{\text{Edd},i} | M_j) \lambda_{\text{Edd},i} d \log \lambda_{\text{Edd}}$, while the corresponding upper and lower limits were calculated as $\sum_i (f(\lambda_{\text{Edd},i}) + \Delta f_i) \lambda_{\text{Edd},i} d \log \lambda_{\text{Edd}}$ and $\sum_i (f(\lambda_{\text{Edd},i}) - \Delta f_i) \lambda_{\text{Edd},i} d \log \lambda_{\text{Edd}}$, where Δf_i is the total error in the interval, including the statistical and systematic (arising when the contribution of the active nucleus to the IR galaxy luminosity is taken into account) ones.

The results of our calculations are presented in Fig. 12 at the top. As we see, within the error limits, the characteristic SMBH growth time does not depend on the galaxy stellar mass and exceeds the lifetime of the Universe at least by several times and may be an order of magnitude (depending on what type of M_{BH} estimates is used).

Subsequently, we calculated τ based on the analytical model of $f(\lambda_{\text{Edd}} | M_*)$. Here, finding $\langle \lambda_{\text{Edd}} \rangle$ runs into a problem when integrating over $\log \lambda_{\text{Edd}}$ in infinite limits, as required by the averaging procedure (22). When integrating to $+\infty$, an exponential cutoff, which lies in the interval $\log \lambda_{\text{Edd}}^* \in (-1.77, -1.58)$ for the rough estimates and $\log \lambda_{\text{Edd}}^* \in (0, 1)$ for the accurate and mixed ones, solves the problem of the divergence of the power-law dependence. The existence of a cutoff at $\log \lambda_{\text{Edd}}^* \in (0, 1)$ is also confirmed by works on the earlier Universe (see, e.g., Aird et al. 2018). As $-\infty$ is approached, the behavior of $f(\lambda_{\text{Edd}} | M_*)$ is unknown, but Fig. 9 shows that this dependence flattens out or at least has a significantly smaller slope at $\log \lambda_{\text{Edd}} < -3$. Hence it can be concluded that

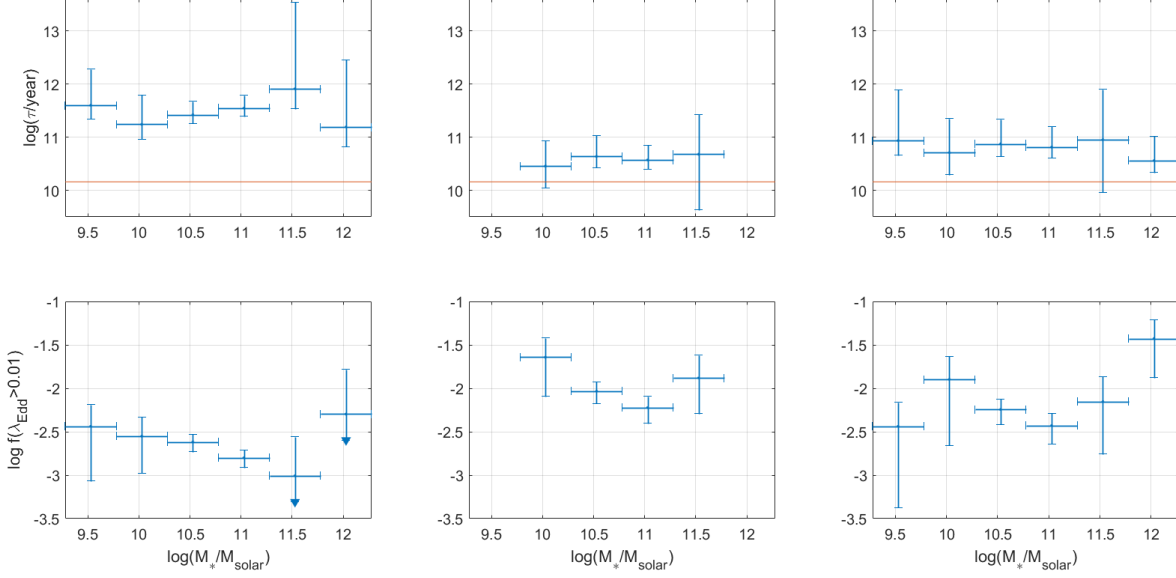


Figure 12. Top: Characteristic SMBH growth time at the present epoch versus galaxy stellar mass when using the rough (left), accurate (center), and mixed (right) SMBH mass estimates in the calculations by assuming the accretion efficiency to be $\eta = 0.1$ (at a different η this time will change proportionally). The horizontal red line corresponds to the Hubble time $t_H = 13.7$ Gyr. Bottom: Duty cycle at the present epoch versus M_* when using the rough (left), accurate (center), and mixed (right) SMBH mass estimates in the calculations. At η different from 0.1 the duty cycle will change inversely proportionally to η .

the value of the integral $\int_{-\infty}^{+\infty} f_{\text{true}}(\lambda_{\text{Edd}}|M_*) \lambda_{\text{Edd}} d \log \lambda_{\text{Edd}}$ lies between $\int_{-3}^{+\infty} f_{\text{model}}(\lambda_{\text{Edd}}|M_*) \lambda_{\text{Edd}} d \log \lambda_{\text{Edd}}$ and $\int_{-\infty}^{+\infty} f_{\text{model}}(\lambda_{\text{Edd}}|M_*) \lambda_{\text{Edd}} d \log \lambda_{\text{Edd}}$, where $f_{\text{true}}(\lambda_{\text{Edd}}|M_*)$ denotes the true distribution of $f(\lambda_{\text{Edd}}|M_*)$ and $f_{\text{model}}(\lambda_{\text{Edd}}|M_*)$ denotes the analytical model based on the λ_{Edd} -constrained data. The uncertainty in $f(\lambda_{\text{Edd}}|M_*)$ at small λ_{Edd} affects significantly the τ estimates based on the analytical model, but the related error does not exceed half an order of magnitude. The uncertainties in the model parameters for $f(\lambda_{\text{Edd}}|M_*)$ make an additional weighty contribution to the error in the τ estimate.

If we take the analytical model (15) with the parameters from Table 5 as a basis, then we will obtain the following results. For the rough M_{BH} estimates $\tau = 3.3 (2.7, 4.8) \times 10^{11}$ years; for the accurate and mixed ones $\tau = 5.2 (4.4, 6.4) \times 10^{10}$ years and $\tau = 0.9 (0.7, 1.1) \times 10^{11}$ years, respectively. Thus, when using the power-law model with an exponential cutoff at large λ_{Edd} , the results being obtained agree well with those obtained above (Fig. 12 at the top) by integrating the discrete function $f(\lambda_{\text{Edd}})$.

Finally, it should be noted that all of the values of τ presented above were obtained by assuming the accretion efficiency to be 10%, corresponding to standard accretion onto a slowly rotating BH (Shakura and Sunyaev 1973). At a different value of the parameter η the characteristic SMBH growth time will change proportionally.

Next, we can calculate, just as was done in Aird et al. (2018), the SMBH “duty cycle”:

$$f(\lambda_{\text{Edd}} > 0.01|M_*) = \int_{-2}^{+\infty} f(\lambda_{\text{Edd}}|M_*) d \log \lambda_{\text{Edd}}, \quad (23)$$

i.e., the fraction of galaxies at the present epoch in which the SMBHs accrete matter with a rate of at least 1% of the critical one (assuming the accretion to proceed via a standard disk).

We estimated $f(\lambda_{\text{Edd}} > 0.01)$ using the discrete dependences $f(\lambda_{\text{Edd}})$ in separate M_* intervals. The results for different types of M_{BH} estimates are shown in Fig. 12. We see that the duty cycle is ~ 0.2 –1% and does not depend, within the error limits, on the galaxy stellar mass.

We additionally estimated the duty cycle $f(\lambda_{\text{Edd}} > 0.01)$ based on the analytical models (15). As a result, $f(\lambda_{\text{Edd}} > 0.01) = 0.2 (0.18, 0.23)\%$, $f(\lambda_{\text{Edd}} > 0.01) = 0.61 (0.53, 0.71)\%$, and $f(\lambda_{\text{Edd}} > 0.01) = 0.44 (0.37, 0.5)\%$ for the rough, accurate, and mixed M_{BH} estimates, respectively. These results agree well with the estimates of $f(\lambda_{\text{Edd}} > 0.01|M_*)$ based on the discrete dependences $f(\lambda_{\text{Edd}})$.

Aird et al. (2018) concluded that $f(\lambda_{\text{Edd}} > 0.01)$ increases with M_* for star-forming galaxies at $z \gtrsim 0.5$. At the same time, no such dependence was detected for galaxies with a low star formation rate (at the same redshifts), except for the decrease in $f(\lambda_{\text{Edd}} > 0.01)$ at $11 < \log(M_*/M_{\odot}) < 11.5$. At redshifts $z < 0.5$ the measurement errors in Aird et al. (2018) do not allow any conclusion about the dependence of the duty cycle on M_* to be reached. However, it can be seen from Fig. 6 in Aird et al. (2018) that at low z for all of the presented M_* $f(\lambda_{\text{Edd}} > 0.01)$ converges to 0.5–1%, in good agreement with our results. Thus, the dependence $f(\lambda_{\text{Edd}} > 0.01|M_*)$ could experience noticeable evolution in the last several billion years.

Note that when the accretion efficiency η differs from 10%, all of the above estimates of the AGN duty cycle change inversely proportionally to η .

6 CONCLUSIONS

In this paper we studied the distribution of accretion rates in AGNs of the local Universe ($z < 0.15$) based on homogeneous (outside the Galactic plane) near-IR (2MASS) and hard X-ray (Swift/BAT) surveys. Using sufficiently accurate SMBH mass estimates allowed us to better estimate the Eddington ratio λ_{Edd} for approximately half of the AGN sample; for the remaining objects we used a less accurate estimate based on the correlation of M_{BH} with the galaxy stellar mass M_* . As a result, we obtained the following results for a wide range of galaxy masses, $9.28 < \log(M_*/M_\odot) < 12.28$, including the most massive galaxies in the local Universe:

- i The distribution $f(\lambda_{\text{Edd}})$ above $\log \lambda_{\text{Edd}} = -3$ is described by a power law with M_* -independent parameters, declining with a characteristic slope ≈ -0.7 up to the Eddington limit ($\log \lambda_{\text{Edd}} \sim 0$), where there is evidence for a break.
- ii We found evidence that at $\log \lambda_{\text{Edd}} < -3$ the dependence $f(\lambda_{\text{Edd}})$ has a lower slope or flattens out.
- iii We estimated the SMBH growth time at the present epoch. It does not depend (within the error limits) on the galaxy stellar mass and exceeds the lifetime of the Universe, but by no more than an order of magnitude.
- iv We estimated the mean SMBH duty cycle (the fraction of objects with $\lambda_{\text{Edd}} > 0.01$) at the present epoch. It does not depend (within the error limits) on M_* either and is 0.2–1%.

These results obtained for the present epoch confirm the trends found in previous studies for the earlier Universe and refine the parameters of the dependence $f(\lambda_{\text{Edd}}|M_*)$ at $z < 0.15$. The revealed universal (weakly dependent on the galaxy stellar mass) pattern of the dependence $f(\lambda_{\text{Edd}})$ probably stems from the fact that the main SMBH growth occurred at early epochs in the life of the Universe, while at present the episodes of mass accretion onto SMBHs are associated mainly with stochastic processes in galactic nuclei rather than with global galaxy evolution processes.

ACKNOWLEDGEMENTS

This study was supported by grant no. 19-12-00396 of the Russian Science Foundation.

REFERENCES

J. Aird, A.L. Coil, J. Moustakas, et al., *Astrophys. J.* **746**, 90 (2012)
 J. Aird, A.L. Coil, A. Georgakakis, et al., *MNRAS* **451**(2), 1892 (2015)
 J. Aird, A.L. Coil, and A. Georgakakis, *Astrophys. J.* **474**(1), 1225 (2018)
 M. Ajello, D.M. Alexander, J. Greiner, et al., *Astrophys. J.* **749**, 21 (2012)
 E.F. Bell, D.H. McIntosh, N. Katz, and M.D. Weinberg, *Astrophys. J. Suppl. Ser.* **799**, 289 (2003)
 M. Bilicki, T.H. Jarrett, J.A. Peacock, et al., *Astrophys. J. Suppl. Ser.* **210**, 9 (2013)
 A. Bongiorno, A. Merloni, M. Brusa, et al., *MNRAS* **427**(4), 3103 (2012)
 A. Bongiorno, A. Schulze, A. Merloni, et al., *Astron Astrophys.* **588**, A78 (2016)
 N.J. Bonne, M.J. Brown, H. Jones, and K.A. Pimbblet, *Astrophys. J.* **799**, 160 (2015)
 L. Ciotti and J.P. Ostriker, *Astrophys. J.* **551**(1), 131 (2001)
 R.M. Cutri, M.F. Skrutskie, S. Van Dyk, et al., *Astrophys. Sp. Sci.* **364**, 1 (2003)

A.C. Fabian, *ARAA* **50**, 455 (2012)
 A. Georgakakis, P.G. Pérez-González, N. Fanidakis, et al., *MNRAS* **440**(1), 339 (2014)
 A. Georgakakis, J. Aird, A. Schulze, et al., *MNRAS* **471**(2), 1976 (2017)
 A.W. Graham and C.C. Worley, *MNRAS* **388**, 1708 (2008)
 J.P. Huchra, L.M. Macri, K.L. Masters, et al., *Astrophys. J. Suppl. Ser.* **199**, 26 (2012)
 T.H. Jarrett, T. Chester, R. Curti, et al., *Astron. J.* **125**, 525 (2003)
 T. Jarrett, *Publ. Astron. Soc. Aust* **21**, 396 (2004)
 M.L. Jones, R.C. Hickox, C.S. Black, et al., *Astrophys. J.* **826**(1), 12 (2016)
 G. Kauffmann and T.M. Heckman, *MNRAS* **397**(1), 135 (2009)
 G. A. Khorunzhev, S. Y. Sazonov, R. A. Burenin, and A. Y. Tkachenko, *Astron. Lett.* **38**, 475 (2012)
 A. King and K. Pounds, *ARAA* **53**, 115 (2015)
 J. Kormendy and L.C. Ho, *ARAA* **51**, 511 (2013)
 M. Koss, B. Trakhtenbrot, C. Ricci, et al., *Astrophys. J.* **850**, 74 (2017)
 E. Laurikainen, H. Salo, R. Buta, and J. H. Knapen, *MNRAS* **381**, 401 (2007)
 E. Laurikainen, H. Salo, R. Buta, et al., *MNRAS* **405**, 1089 (2010)
 P. Madau and M. Dickinson, *ARAA* **52**, 415 (2014)
 J. Magorrian, S. Tremaine, D. Richstone, et al., *Astron. J.* **115**, 2285 (1998)
 A. Malizia, S. Sazonov, L. Bassani, et al., *New Astron.*, (2020)
 E.J. Marchesini, N. Masetti, E. Palazzi, et al., *Astrophys. Sp. Sci.* **364**, 1 (2019)
 T.P. Martinsson, M.A. Verheijen, K. B. Westfall, et al., *Astron Astrophys.* **557**, A131 (2013)
 T. Di Matteo, V. Springel, and L. Hernquist, *Astron. J.* **433**(7026), 604 (2005)
 S.S. McGaugh and J.M. Schombert, *Astron. J.* **148**, 77 (2014)
 A. Merloni and S. Heinz, *MNRAS* **388**(3), 1011 (2008)
 S.S. Murray, A. Kenter, W.R. Forman, et al., *Astrophys. Sp. Sci.* **161**, 1 (2005)
 T. Naab and J.P. Ostriker, *ARAA* **55**, 59 (2017)
 K. Oh, M. Koss, C.B. Markwardt, et al., *Astrophys. J. Suppl. Ser.* **235**, 4 (2018)
 S. Sazonov, J.P. Ostriker, L. Ciotti, and R.A. Sunyaev, *MNRAS* **358**(1), 168 (2005)
 S. Sazonov, S.P. Willner, A.D. Goulding, et al., *Astrophys. J.* **757**, 181 (2012)
 N.I. Shakura and R.A. Sunyaev, *Astron Astrophys.* **24**, 337 (1973)
 F. Shankar, D.H. Weinberg, and J. Miralda-Escude, *Astrophys. J.* **690**(1), 20 (2009)
 M.F. Skrutskie, R.M. Cutri, R. Stiening, et al., *Astron. J.* **131**, 1163 (2006)
 S. Tremaine, K. Gebhardt, R. Bender, et al., *Astrophys. J.* **574**(2), 740 (2002)
 J. Tueller, R.F. Mushotzky, S. Barthelmy, et al., *Astrophys. J.* **681**, 113 (2008)
 R.B. Tully, H.M. Courtois, and J.G. Sorce, *Astron. J.* **152**, 50 (2016)
 Y. Ueda, M. Akiyama, G. Hasinger, and M. G. Watson, *Astrophys. J.* **786**(2), 104 (2014)
 C.N.A. Willmer, *Astrophys. J. Suppl. Ser.* **236**, 47 (2018)